though the refractive index does not yet change and certainly does not decrease [25].

Since the apparent blue-shift is the result of interference involving light escaping from the cavity, we verify the magnitude of the apparent blue-shift by calculating it for cavities with a decreased escaping intensity from the top mirror. Therefore, we have performed calculations for cavities with sequentially increased number of top Bragg layers as shown in Fig. 2(b). With increasing number of top layers the cavity becomes more symmetric and at the same time the quality factor of the cavity increases. In Fig. 2(b) we observe that the apparent blue shift of the cavity resonance at $\Delta t < 0$ decreases for increasingly symmetric cavities. In Fig. 2(b) the red shift of the cavity resonance at $\Delta t = 0$ decreases with increasing quality factor, which will be discussed in section 3.3. We summarize our observations that the reversible red shift of the cavity resonance corresponds to the derived electric Kerr effect, whereas the apparent blue-shift is the result of an spatial interference.

Fig. 2. (a) Measured (symbols) and calculated (red curve) resonance frequency versus time delay (Δt) between pump and probe for a GaAs/AlAs cavity ($Q = 390 \pm 60$). The resonance frequency red-shifts due to increased refractive index only near temporal overlap ($\Delta t = 0 \pm 15\ fs$) of pump-probe, shown with dashed curve. (b) Calculated spectra for a GaAs/AlAs cavity that consists of 19 pairs of bottom Bragg layers, $\lambda-$layer, and sequentially changed number of layers on the top Bragg mirror.

3.2. The effect of the backbone's electronic bandgap

To compare the effect of the backbone's electronic bandgap we have performed Kerr switching experiments on cavities that has similar quality factors and consist of GaAs/AlAs ($Q = 390$) and AlGaAs/AlAs ($Q = 210$). Figure 3(a) and 3(c) shows the resonance frequency versus time delay for these GaAs/AlAs and AlGaAs/AlAs microcavities, respectively. The cavity resonance for the AlGaAs cavity shifts by 1.8 cm^{-1}, which is less than 4.7 cm^{-1} of the GaAs cavity. To understand this lower frequency shift with the AlGaAs/AlAs cavity we consider how the third order susceptibility depends on material parameters.

Figure 4 shows the nondegenerate dispersion (G_2) curve of the electronic Kerr effect for probe frequency ω_{pr} within the original (O) and conventional (C) telecom bands. The function G_2 determines the dispersion of the nonlinear index coefficient n_2 as follows [26]:

$$n_2(\omega_{pr}, \omega_{pu}) = \frac{\hbar c K}{2} \frac{\sqrt{E_p}}{E_{gap}^4 n_{0pr} n_{0pu}} G_2(\omega_{pr}, \omega_{pu}), \tag{1}$$

where K is a constant, E_p the Kane energy ($\simeq 21\ eV$), E_{gap} the bandgap, and n_{0pr}, n_{0pu} are the linear refractive indices at probe (ω_{pr}) and pump frequency (ω_{pu}), respectively. The dispersion function is obtained by the Kramers-Kronig transformation of the interband absorption

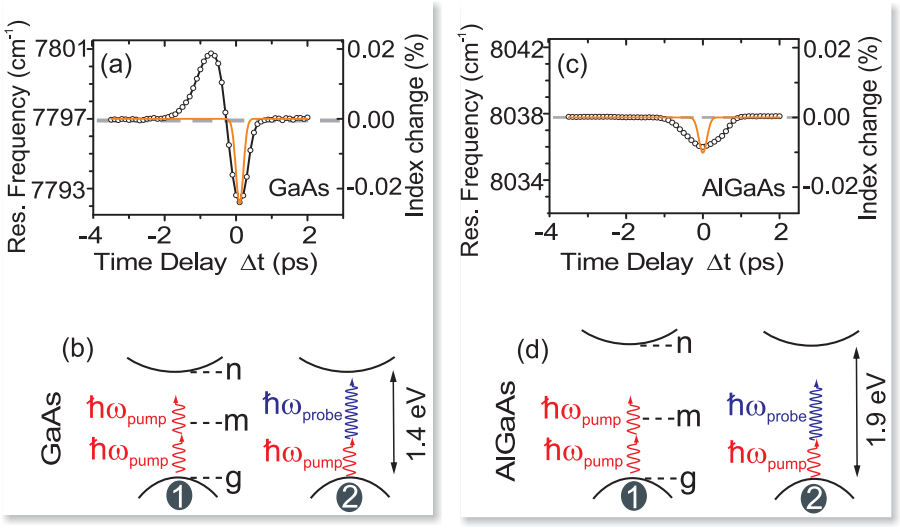

Fig. 3. Resonance frequency versus time delay (Δt) between pump and probe for (a) GaAs/AlAs ($Q = 390$) and (c) AlGaAs/AlAs cavity. The resonance frequency red-shifts due to increased refractive index only near temporal overlap ($\Delta t = 0 \pm 15\ fs$) of pump-probe. Both cavities are switched at 65 pJ/μm^2 pump fluence. The dashed lines represent the unswitched cavity resonance frequency. The solid curves represent the induced refractive index change. The schematic representation of the electronic bandgap of (b) GaAs and (d) AlGaAs and the energy of the pump and probe photons relative to the bandgap.

change [26]. The dispersion of the nonlinear refractive index coefficient n_2 has been also validated experimentally [27–30]. We calculate the dispersion function G_2 from Sheik-Bahae et. al. [26], Table 2. In Fig. 4 we see that the nonlinear index coefficient is maximized near the non-degenerate two photon absorption edge [28,29]. Our cavities are designed to operate within the original (O) telecom band, which corresponds to a reduced probe frequency $\hbar\omega_{pr}/E_{gap} = 0.65$. We set the pump frequency to $\hbar\omega_{pu}/E_{gap} = 0.35$ in order to suppress degenerate free carrier excitation, see Fig. 3(b1). The non-degenerate free carrier excitation (pump and probe, Fig. 3(b2)) is suppressed since the probe fluence is much smaller than the pump fluence. At this setting of the pump frequency, the non-degenerate sum of pump and of probe frequency are tuned close to the electronic bandgap of the material. As a result, the nonlinear index coefficient is close to the maximum, as shown in Fig. 4. We use the same frequency of the pump and of the probe light for the AlGaAs/AlAs cavity. In this case we operate away from the electronic bandgap of AlGaAs both for degenerate two-pump photon excitation (Fig. 3(d1)) and for non-degenerate pump and probe photon excitation (Fig. 3(d2)). Consequently, we observe less refractive index change due to a smaller nonlinear refractive index coefficient, see Fig. 4, which explains the smaller shift of the cavity resonance in Fig. 3(c).

Figure 4 also shows the dependence of the nonlinear index coefficient versus pump frequency when the cavity resonance ω_{pr} is set to operate within the C-band ($1530 - 1565$ nm). In this case, we see that the electronic Kerr effect is maximized when the pump frequency is tuned to $\hbar\omega_{pu}/E_{gap} = 0.5$ ($\lambda_{pu} \simeq 1700$ nm for GaAs). At this pump frequency, however, the probability for the excitation of free carriers via two pump photons will be strong, which will hinder the electronic Kerr effect [18]. In contrast, cavities operating within O-band ($1260 - 1360$ nm) are more amenable than in the C-band for ultrafast switching using the electronic Kerr effect, since the greater probe frequency can be combined with a lower pump frequency to profit from

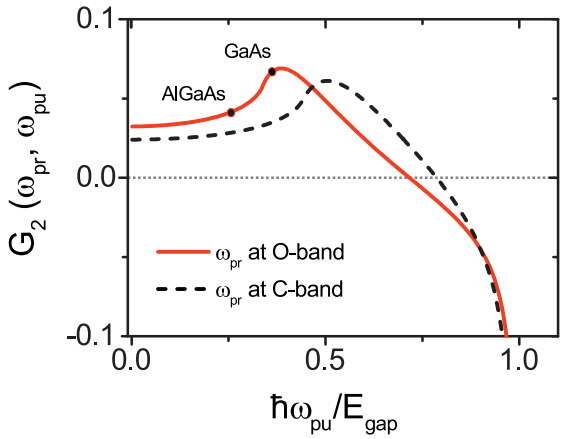

Fig. 4. Nondegenerate dispersion curve of the electronic Kerr effect for probe frequency within original (O) and conventional (C) telecom bands, shown with solid and dashed curves, respectively. The symbols mark the G_2 values at our setting of pump frequency for GaAs and AlGaAs cavities.

the maximized nonlinear index. Simultaneously, a lower pump frequency will much less likely induce unwanted two-photon excitation of free carriers.

3.3. The effect of the cavity storage time

We have performed switching experiments on cavities with different quality factors to investigate the effect of the cavity storage time τ_c on the Kerr-induced resonance frequency change. Figure 5 shows the relative cavity resonance frequency shift versus both the quality factor Q and the storage time τ_c of the cavity. We observe that the shift of the cavity resonance frequency ($\delta\omega$) relative to the cavity linewidth ($\Delta\omega$) is maximal when the storage time is matched to the pump pulse duration τ_P. We see both in our measurements and in our model (for the model see Appendix B) that increasing the storage time τ_c of the cavity not only decreases the switching speed but also decreases the induced frequency shift induced via the Kerr effect. This can be understood since the magnitude of the observed frequency shift ($\delta\omega$) is given by the time-overlap integral of the pump and probe light that is stored in the cavity [17]. The decreasing frequency shift with increasing quality factor is caused by the decreased temporal overlap of pump and probe as the cavity-stored probe pulse becomes much longer than the pump pulse ($\tau_{cav} \gg \tau_P$).

In qualitative agreement with our experiments, our model in Fig. 5 shows that a greater resonance frequency shift is observed for a cavity that matches the switch pulse duration during the Kerr switching of a cavity. The relative shift of the resonance frequency is maximal at $\tau_c = 140$ fs, reaching a value close to 40%, when the duration of the cavity-stored probe matches the pump duration ($\tau_c \simeq \tau_P$). Our model predicts a greater resonance frequency shift compared to our experiments. Our model employed in Fig. 5 is an improvement over our earlier work since it contains explicit time dependency, as opposed to the time-independent model we presented earlier [18]. In our previous study [18] we have investigated the effect of the cavity enhancement and found that the effect of the counteracting free carriers is more pronounced for high quality factor cavities. In a cavity with a high quality factor the probe light intensity is enhanced and thereby the probability of degenerate and non-degenerate two-photon excitation of free carriers is increased [18]. Therefore, the difference between our dynamic model and our experiments is larger for high quality factor cavities since we can currently not include free carrier effects in

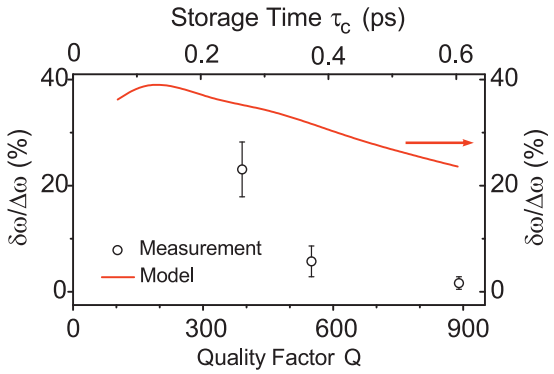

Fig. 5. Relative cavity resonance frequency change versus quality factor and cavity storage time. The calculations and the experiments are performed at 65 pJ/μm^2 pump fluence and pulse duration $\tau_{pu} = 140$ fs. The calculations are performed at pump-probe delay $\Delta t = -100$ fs. Black circles show the measured results within the standard deviation. The solid curve indicates the calculated relative frequency change for different quality factor cavities.

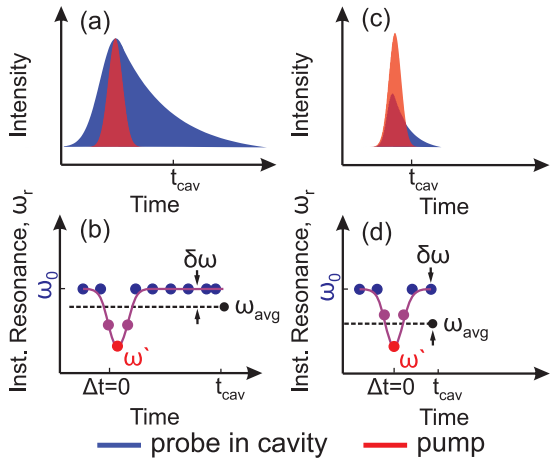

Fig. 6. Schematic representation of the pump and probe pulses in the cavity for two different quality factor cavities, (a) high-Q, (c) low-Q. The lower panels show the instantaneous frequency shift versus time. The cavity resonance instantaneously shifts from ω_0 to ω' at pump probe overlap ($\Delta t = 0$). The detected resonance shift (ω_{avg}) is deduced from the transient reflectivity that is a result of the time averaging of the cavity storage and detector response time. A larger resonance frequency shift $\delta\omega$ is observed for cavities with shorter storage times.

the model. In cavities with a short storage time the excited free carrier density is reduced and the temporal overlap of the pump pulse with the cavity-stored probe light is increased ($\tau_c \simeq \tau_P$), which even allows to Kerr switch a cavity resonance at exhilarating THz clock rates [20].

Figure 6 schematically illustrates the effect of the storage time of the cavity on the Kerr switching of a microcavity in real time. We plot situations where the delay Δt is such that the overlap of the pump and cavity-stored probe is maximal, and we assume the observed cavity resonance ω_{avg} to be averaged over the whole pulse duration in view of the relatively slow detection ($t_{int} > \tau_{pr}$), see section 2.2. For a high quality factor cavity, see Fig. 6(a) and 6(b),

there is no pump light during a long fraction of the probe pulse in the cavity since $\tau_c \gg \tau_P$. As a result, the average resonance frequency shift ω_{avg} is small. Given the same refractive index change, one would naively expect to observe a greater relative shift of the cavity resonance for a high quality factor cavity. However, this is only true if the switch duration is longer than the cavity storage time ($\tau_c < \tau_P$). Since the Kerr switching of the cavity is performed within the pump pulse duration, one has to consider the overlap integral in time to get the average resonance frequency shift. This overlap is determined both by the duration of the pump pulse and the quality factor of the cavity that affects the duration of the cavity-stored probe pulse. Consequently, at similar switch conditions a cavity with a shorter storage time will reveal a greater shift of the time averaged resonance ω_{avg} since the instantaneous cavity resonance shift ω' has a larger weight. As illustrated in Fig. 6(c) and 6(d), a larger portion of the cavity-stored probe light overlaps with the short pump pulse in a cavity that has a short storage time, close to the pump pulse duration ($\tau_c \simeq \tau_P$).

3.4. The effect of the pump pulse duration

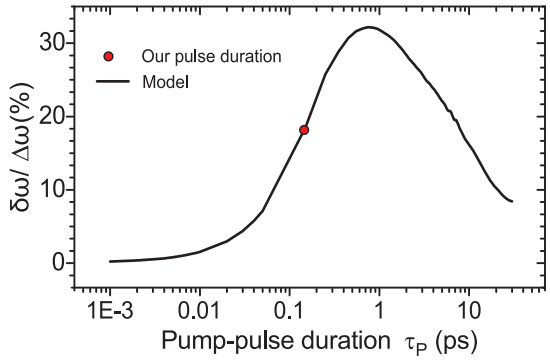

Fig. 7. Calculated relative cavity resonance frequency change with respect to the cavity linewidth ($\Delta\omega$) versus the pump pulse duration for GaAs/AlAs cavity with $Q = 450$. The calculations are performed at a pump intensity of 70 GW/cm^2 and the peak intensity is kept constant for each pulse duration. The calculations are performed at pump-probe delay $\Delta t = 0$ fs. The red circle marks the duration of the pump pulse in our experiments.

To investigate the effect of the pump pulse duration on Kerr-induced cavity resonance frequency switching, we have performed calculations on a switched cavity using our dynamic model as a function of the pump pulse duration. Similar to our experiments, the microcavity in our calculations has 7 pairs of GaAs/AlAs layers in the top mirror and 19 pairs of GaAs/AlAs layers in the bottom mirror and is surrounded by air. For the modeled nanostructure we get a quality factor $Q = 450$ in our calculations whereas the closest cavity in our experiments has a quality factor $Q = 390$. The difference in measured and calculated quality factors are due to absence of loss mechanisms in the model, such as slight deviations of the layer thicknesses versus the nominal design. Moreover, in our model we do not include the GaAs wafer that also increases the quality factor, given the increased contrast between air and the bottom Bragg mirror. Figure 7 shows the cavity resonance frequency shift relative to the resonance linewidth ($\delta\omega/\Delta\omega$) versus the pump pulse duration at a pump-probe delay $\Delta t = 0$ fs. The maximum shift ($\delta\omega$) reaches 32% when the pump pulse duration is set to $\tau_P = 550$ fs for this particular cavity. Beyond $\tau_P = 1$ ps the cavity resonance frequency shift decreases with increasing pump pulse duration. When we compare the optimum pump pulse duration ($\tau_P = 550$ fs) to the cavity storage time ($\tau_c = 300$ fs for $Q = 450$, see Fig. 5) we observe that they are of comparable mag-

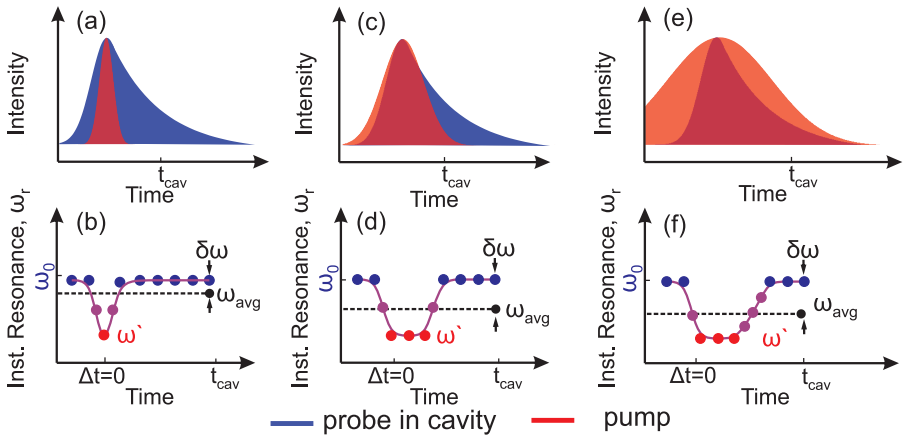

Fig. 8. Schematic representation of the pump and probe pulses in the cavity for three different pump pulse durations. The peak intensity of the pump pulse is kept constant while stretching the pump pulse. The lower panels show the instantaneous frequency shift versus time. The cavity resonance instantaneously shifts from ω_0 to ω' at pump probe overlap ($\Delta t = 0$). The detected resonance shift (ω_{avg}) is deduced from the transient reflectivity that is a result of the time averaging of the cavity storage and detector response time.

nitude, as is to be expected. It is noteworthy that the times are not exactly equal as $\tau_P/\tau_c = 1.8$. The difference of unity is probably related to subtle issues of pulse shapes that determine the detailed temporal overlap of the pump and probe fields. Although, the effect of the cavity storage time is similar to pump pulse duration we see in Fig. 7 that at $\tau_P = 140$ fs the resonance frequency shift is smaller than the results shown in Fig. 5. This is because in Fig. 5 the resonance frequency shift is calculated $\Delta t = -100$ fs, at which delay the resonance frequency shift reaches its maximum [20], whereas at $\Delta t = 0$ fs the resonance shift is smaller on the probe pulse has already partially escaped from the cavity. This time delay was chosen here so that we can calculate the effect of the pump pulse duration that is shorter than the cavity storage time.

To interpret the behavior versus pulse duration, we schematically depict in Fig. 8 the probe pulse that is in resonance with the cavity and the pump pulse versus real time. The resonance frequency of the cavity shifts from ω_0 to ω' due to the instantaneous change of the refractive index. Given the time averaging of the detector, we observe an average resonance frequency shift ω_{avg} that is smaller than the instantaneous shift. For a short pump pulse duration ($\tau_P < \tau_c$) illustrated in Fig. 8(a) the cavity-averaged frequency shift is small, see Fig. 8(b). As the pump pulse gets longer in time (Fig. 8(c)) the weight of instantaneous shift increases in the time-averaged resonance frequency shift. As a result, a greater shift of the cavity resonance is observed, see Fig. 8(d). Stretching the pump pulse to be much longer than the cavity storage time tomographically samples the probe light in the cavity, see Fig. 8(e) and 8(f). The average resonance frequency shift decreases when $\tau_P \gg \tau_c$ since the magnitude of the frequency shift $\delta\omega$ is given by the overlap integral of the pump and probe. We conclude that the storage time of the cavity and the duration of the pump pulse have similar consequences in resonance frequency shift of the cavity [17].

Our dynamic calculations have shown that the relative resonance frequency shift can be increased by 1.7×, by increasing the pump pulse duration from $\tau_P = 140$ fs to $\tau_P = 550$ fs. As a result, we project that the resonance frequency shift we experimentally obtain 5.6 cm^{-1} can be increased to 9.5 cm^{-1}, which is half a linewidth.

4. Summary and conclusion

We have studied the ultrafast all-optical switching of GaAs/AlAs and AlGaAs/AlAs semiconductor microcavities at telecom wavelengths using the electronic Kerr effect. We investigate the effect of the pump pulse duration, the cavity storage time, backbone material, and the frequency of the pump and the probe relative to the electronic bandgap of the backbone material. We show that the refractive index change induced by the electronic Kerr effect is increased when the cavity storage time match the pump pulse duration. Our results indicate that cavities with AlGaAs backbone hold the advantage that both the pump and the probe can be at telecom wavelengths. In this case, for a cavity operating at *O*-band, the pump frequency should be set to about 7280 cm^{-1}(1370 nm) to maximize the non-degenerate nonlinear index coefficient. Two-photon excitation of free carriers via degenerate pump photons will still be suppressed at this photon energy since AlGaAs has a larger bandgap. Our results indicate that an additional twofold increase of the nonlinear index coefficient can be expected with this setting of the cavity resonance and the pump frequency for AlGaAs cavity.

Appendix A: Transient reflectivity

We explain the transient reflectivity using the description given in earlier studies [23, 31, 32]. In the absence of spectral filtering, the measured signal J, neglecting electronic amplification factors, is equal to the magnitude of the time- and space-integrated Poynting vector S [23, 31]:

$$J = \pi r^2 \int_{-t_{int}/2}^{t_{int}/2} |S| dt = \int_{-t_{int}/2}^{t_{int}/2} \sqrt{\frac{\varepsilon_0}{\mu_0}} E(t)^2 dt \quad (2)$$

$$\approx \pi r^2 \sqrt{\frac{\varepsilon_0}{\mu_0}} \frac{\tilde{E}_0}{2} \int_{-\infty}^{\infty} (e^{-4ln2t^2/\tau_P^2})^2 dt \quad (3)$$

$$= \pi r^2 \sqrt{\frac{\varepsilon_0}{\mu_0}} \sqrt{\frac{\pi}{2ln(2)}} \frac{\tau_P \tilde{E}_0^{\,2}}{4}, \quad (4)$$

where the electric field E(t) reflected by a mirror onto the detector can be separated in a Gaussian envelope $\tilde{E}(t)$ of FWHM τ_P and amplitude $\tilde{E}_0$ that is multiplied by sinusoidal component with a carrier frequency ω_0 in rad/s. This slowly varying envelope approximation (SVEA, see [33]) can be applied to pulses where $\tau_P >> 1/\omega_0$, and where ω_0 does not change over t, in other words, for bandwidth limited pulses. For pulses whose envelope is broadened by the interaction with a cavity, the analytic expression (Eq. (4)) is not valid, but the approximation of the integration limits remains the same. The beam is collimated and has radius r, ε_0 and μ_0 denote the permitivity and permeability of free space, respectively. Since the integration time t_{int} of the InGaAs line array detector is much longer than any probe interaction time τ_{pr}, we essentially integrate all probe light that is stored or reflected by the cavity, given a pump-probe time delay Δt. The probe interaction time is either $\tau_{pr} = \tau_P$ or $\tau_{pr} = Q/\omega_0$, whichever is greater, and it is in the 100 fs to 1 ps range. Therefore, the boundaries of time integral in Eq. (2) can be taken to be infinity because $t_{int} >> \tau_P$. The squared oscillating term can then be integrated separately and yields $1/2$. In Eq. (3) we approximate the peak intensity for a focussed Gaussian pulse as $I = 4\sqrt{ln2}G/(\pi^{3/2} r^2 \tau_P)$, where r is the waist radius at the focus and G the energy per pulse. Eq. (3) reveals that it is not the instantaneous transmission or reflection that is measured, but the integrated intensity.

In our study, we use a spectrometer to frequency resolve the reflected transient signal. The reflected signal from the cavity is spectrally filtered with a spectrometer (Acton) and detected with a nitrogen cooled InGaAs line array detector (Princeton Instruments). Therefore, the observed

spectrum, without amplification and conversion factors, is a Fourier transform of $E(t)$ [31,32]

$$J(\omega) = \pi r^2 (\varepsilon_0 c)^{-1} \left| \int_{-\infty}^{\infty} dt E(t) e^{i\omega t} \right|^2 \tag{5}$$

where c is the velocity of light in free space. The field escaping from a cavity whose resonance frequency shifts in time may exhibit new frequency components where the amplitude is higher than that of the incident bandwidth limited pulse. In this case, the ratio of the reflected pulse to the reference pulse, called the transient reflectivity $R^t(\omega) = J(\omega)_{sample}/J(\omega)_{ref}$ exceeds unity at the new frequency components. In this sense, the transient reflectivity differs from the reflectivity measured in a CW experiment that is necessarily always bounded to 100%. The measured transient reflectivity $R^t(\omega)$ is a result of the probe light that impinges at delay Δt, circulates in the cavity during on average the storage time τ_c, escapes, and is then integrated by the detector. Therefore, we call the measured signal the transient reflectivity or the transient transmission.

Appendix B: Model to calculate time-resolved spectra

The model that we employ to calculate the time-resolved transient reflectivity R^t spectra has previously been introduced by by Harding et. al. [25]. The probe field is calculated in the time domain at every position in a one-dimensional planar microcavity that experiences a time-dependent refractive index. To account for the induced refractive index change $n(t)$, we consider here the positive non-degenerate Kerr coefficient of GaAs [18]. We start with a Gaussian probe pulse at position $z = z_0$:

$$E_{pr}(z_0,t) = E_0(z_0) e^{-i\omega t} e^{-(t-t_0/\tau_{pr})^2}, \tag{6}$$

where E_0 is the amplitude of the probe field E_{pr} and ω the angular frequency, t running time and t_0 is the launch time of the probe pulse. In our calculations we chose a short duration for the probe pulse ($\tau_{pr} = 10$ fs) to obtain a broad spectral bandwidth and thus a flat response within the spectral region of the cavity resonance. The field that starts from position $z = z_0$ travels in homogeneous medium with a time dependent refractive index $n(t)$. The time that it takes for the field to travel from position z_0 to z is then equal to $t = n(t) \cdot (z - z_0)/c$. As a result, the Gaussian pulse at position z is given by

$$\begin{aligned} E_{pr}(z,t) \quad &= E_{pr}(z_0, n(t) \cdot (z - z_0)/c) \\ &= E_0(z_0) e^{i\omega(n(t)\cdot(z-z_0)/c)} e^{-((n(t)\cdot(z-z_0)/c) - t_0/\tau_{pr})^2}. \end{aligned} \tag{7}$$

Similar to our experiments the structure that we describe in our model consists of air, the top Bragg mirror, the λ-layer, the bottom Bragg mirror, and air after the cavity structure, as shown in Fig. 9. Since the thickness of the GaAs wafer is not exactly known, we exclude it in our model. The Bragg mirrors consist of AlAs and GaAs layers with unswitched refractive indices n_{AlAs} and n^0_{GaAs}, respectively. During the switching of our microcavity we take the refractive index of AlAs and air to be constant in time, whereas the refractive index of GaAs is time dependent. Since the change of the refractive index of AlAs is five times smaller [15] we safely treat its refractive index as a constant. The refractive index of GaAs changes with the time delay Δt between the pump and the probe pulses due to the electronic Kerr effect. Hence, we define a position- and time-dependent refractive index for the structure as follows:

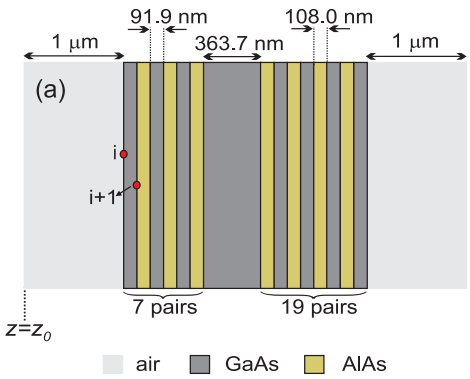

Fig. 9. Schematic picture of the one-dimensional microcavity considered in our model calculations. The Bragg mirrors consist of GaAs and AlAs layers and the λ-layer consists of GaAs. The thickness of the air, GaAs, and AlAs layers are indicated in the figure so as to yield a resonance frequency as in our experiment. The first two interfaces are marked with the indices i and i+1. The probe field is launched at $z = z_0$.

$$n(z,t) = \begin{cases} n_{air} & \text{, z in air} \\ n_{AlAs} & \text{, z in AlAs} \\ n^0_{GaAs} + \frac{12\pi^2\chi^{(3)}}{(n^0_{GaAs})^2 c} \cdot [I_{pu} e^{-(\frac{t-\Delta t}{\tau_{pu}})^2}] & \text{, z in GaAs,} \end{cases} \tag{8}$$

where $\chi^{(3)}$ is the third-order susceptibility of GaAs, I_{pu} the peak intensity of the pump pulse, τ_{pu} the duration of the pump pulse, and Δt the time delay between pump and the probe. In our calculations we neglect the refractive index change induced by the probe light since the intensity of the probe is much lower than the pump intensity. Since the probe field propagates through the microcavity structure that consists of many different materials with different refractive indices, the field encounters many interfaces. The field that impinges on an interface is partly reflected and partly transmitted, as given by the Fresnel coefficients [34]. The reflected ($\mathfrak{r}$) and transmitted ($\mathfrak{t}$) amplitude coefficients at normal incidence from any interface are equal to

$$\begin{aligned} \mathfrak{r} &= \frac{n_1(z,t) - n_2(z,t)}{n_1(z,t) + n_2(z,t)}, \\ \mathfrak{t} &= \frac{2n_1(z,t)}{n_1(z,t) + n_2(z,t)}, \end{aligned} \tag{9}$$

where $n_1(z,t)$ and $n_2(z,t)$ are the time-dependent refractive indices of the first and the second medium, respectively. Due to the transmission and reflection from an interface, there are fields travelling in opposite directions. Part of the field transmitted by interface i is reflected from the next interface $i+1$ and thus interferes with the incident field. As a result, at a given position z inside the microcavity, the field is equal to

$$\begin{aligned} \mathscr{E}^i_{pr}(z,t) \qquad &= E^+_{pr}(z_0, n(z,t) \cdot (z - z_0)/c) \cdot \mathfrak{t}^i \\ &+ E^-_{pr}(z_0, n(z,t) \cdot (z - z_0)/c) \cdot \mathfrak{r}^{i+1} \end{aligned} \tag{10}$$

For convenience we take the direction of the transmission as the positive direction. Since the microcavity structure consists of N interfaces, we have generalized Eq. (10) to N total number of interfaces and mark Fresnel coefficients $\mathfrak{r}^i$ and $\mathfrak{t}^i$ with the index i, which represent the interface number.

We calculate the field at any position z in the multilayer structure by inserting the time-dependent refractive index of GaAs and the time-independent refractive indices of AlAs and air in $n(z,t)$ from Eq. (8) into Eq. (10). Equation (10) can be generalized to a case where both the refractive indicies of GaAs and AlAs are time-dependent. If the field is, for instance, at GaAs and AlAs interface, the time-dependent index of GaAs and AlAs should be inserted in $n_1(z,t)$ and $n_2(z,t)$ in Eq. (9), respectively. To calculate the transient reflectivity spectrum we include all interfaces, see Fig. 9, to obtain the total time-resolved field $\mathscr{E}_{pr}(z,t)$. Next, we perform a discrete Fourier transform on such a field in reflection geometry

$$|\mathscr{E}_{pr}(z,\omega)|^2 = \left| \sum_0^t \mathscr{E}_{pr}(z,t) \cdot e^{-(i2\pi\omega\delta t)} \right|^2. \tag{11}$$

to obtain the transient field $\mathscr{E}(z,\omega)$, and thereby the transient reflectivity R^t spectra. In Eq. (11) δt represents the time step.

Acknowledgments

We thank Allard Mosk and Henri Thyrrestrup for useful discussions. This research was supported by FOM-NWO, the NWO-Nano program, ERC-Pharos Project No. 279248, and STW.